DIRAC Note 2005-02

Pion multiple Coulomb scattering in the DIRAC experiment

A.Dudarev, V.Kruglov, L.Kruglova, M.Nikitin
Laboratory of Nuclear Problems,
Joint Institute for Nuclear Research.

(prepared by V.Kruglov)

Preface

This note is prepared not in usual article style, which means that it does not include full needed information, proof of all statements, complete description of the experiment and even **References**. The note has the main aim to make available the final experimental information about pion multiple scattering in the DIRAC setup. Certainly, the full information is available, but due to its large amount, it takes a lot of time to prepare usual scientific note. Of course, it will be made in the future.

1 Introduction

The knowledge of the multiple scattering of pions in the DIRAC setup elements, especially in the target, plays a crucial role in the DIRAC experiment. An essential part of systematic error in the experiment originates from uncertainties in the description of multiple scattering. The modern experimental status of the multiple scattering in a "thin" samples, presented in scientific literature, does not allow to describe multiple scattering with necessary precision.

This note is the first attempt to study multiple scattering in the frame of the DIRAC experiment. Experimental data presented in the note were collected in the DIRAC run2003.

Six samples prepared for the measurement were equivalent to Ni-target, Al-window, $MSGC$, SFD-$X(Y)$, SFD-W and IH and had exactly the same composition as the real parts of the setup. Size of each sample was about $100 \times 25 mm^2$. All samples were placed just after $DC3$ module in the $T2$- spectrometer arm (see Fig. 1).

Two peculiar features of the experiment define our procedure: 1) Contrary to all other multiple scattering measurements, in our case particles crossing the samples do not have fixed momentum value, but belongs to the momentum range $(1.5 - 2.5) GeV/c$; 2) Due to very small thickness of the samples, in most cases the scale of multiple scattering is comparable with the DC-system resolution, and in case of IH is much smaller. For the latter reason it was impossible to determine multiple scattering in the IH-sample with required accuracy ($\sim 1\%$).

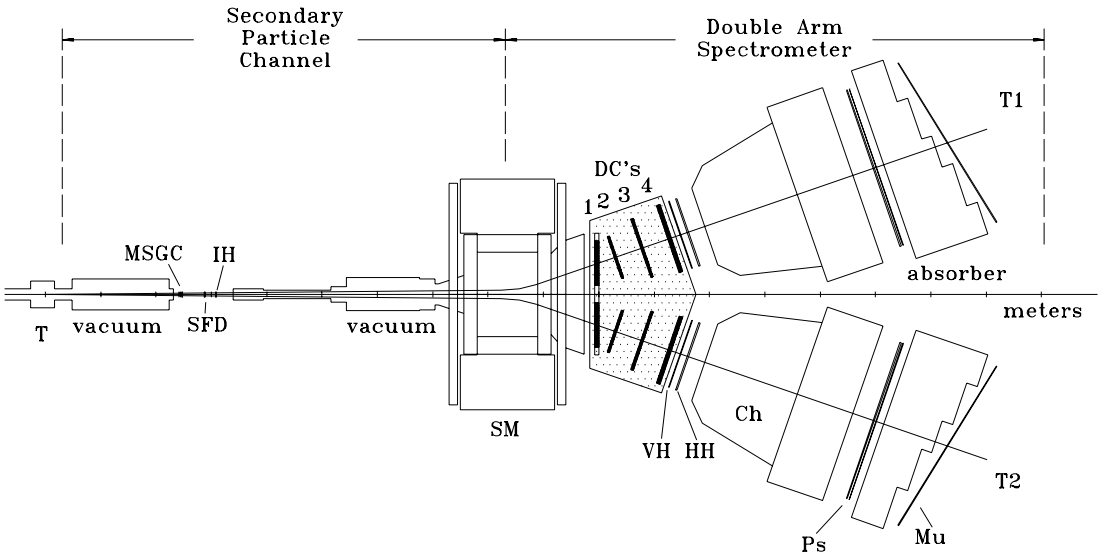

Figure 1: Experimental setup of the DIRAC experiment: T - target station, $MSGC$ - micro-strip gas chambers, IH - ionization hodoscopes, SM - spectrometer magnet, DC - drift chamber system, VH - vertical hodoscopes, HH - horizontal hodoscopes, Ch - Cherenkov counters, Ps - preshower detectors, Mu - muon scintillation counters, $T1$ and $T2$- spectrometer arms.

The plane projected angle (θ) between the two parts of a track, before and after the sample plane, was used in the analysis. The first part of the track was reconstructed in $DC1$-$DC3$ modules. The second part of this track was defined by the crossing point of the first track part with the sample plane and by coordinates detected in the $DC4$ module. The tracking procedure was deeply tested, to be sure in unbiased result.

Distortion of tracks crossing the samples depends on multiple scattering in the samples and the accuracy of the DC-system, and distortion of tracks crossing the sample plane in the vicinity of the corresponding sample depends only on accuracy of the DC-system. Using projected angle distributions for these two kinds of events, it is possible to obtain the pure multiple scattering distribution. It is well known in mathematics , that this procedure is so-called the "ill-posed problem". To solve this problem, some kind of regularization procedure is needed. We used the statistical regularization method, which is the most attractive in our case, because our experimental data are statistical ones by nature. In addition, this method provides not only solution of the problem, but gives the accuracy value of the result.

Below we present:

- Multiple scattering measurement analysis based on the Moliere theory
- Multiple scattering experimental data analysis
- Multiple scattering experimental data fit.

2 Multiple scattering analysis with the Moliere theory

All steps of our procedure were tested with simulated events generated according to the Moliere theory of multiple scattering, because this theory is the most widely used for simulation. Standard Moliere code from the GEANT package was slightly modified. The Fano correction, which introduces in the theory the scattering on atomic electrons, was implemented. Also some code internal tables were extended to make the routine more suitable for very thin samples.

As mentioned in **Introduction**, particles crossing the samples belongs to the momentum range $(1.5 - 2.5)GeV/c$. This makes impossible to perform analysis for any particular momentum with reasonable statistics. Fortunately, a theoretical treatment of the Moliere theory shows momentum independence of the multiple scattering distribution with respect to $\theta \times p$ variable for the DIRAC momentum range. To confirm this statement, the $\theta \times p$-distribution was simulated for four momentum ranges $(1.6 - 1.8 - 2.0 - 2.2 - 2.4)GeV/c$, according to the experimental momentum distribution. The result for Ni-sample is presented in Fig. 2. It is seen the perfect coincidence of the distributions. In the next section this statement is illustrated on experimental data.

In **Introduction** the statistical regularization method was mentioned. Correctness of our procedure for extraction of pure multiple scattering distribution from the data is illustrated in Fig. 3. In this figure the a-distribution was simulated according to the Moliere theory, the b-distribution presents the experimental DC-system resolution, c-distribution is a convolution of the a- and b-distributions and

corresponds to the tracks going through the sample. The reconstructed pure multiple scattering distribution presented in the d-box must be compared with the initial distribution in the a-box. Perfect coincidence of the distributions is evident.

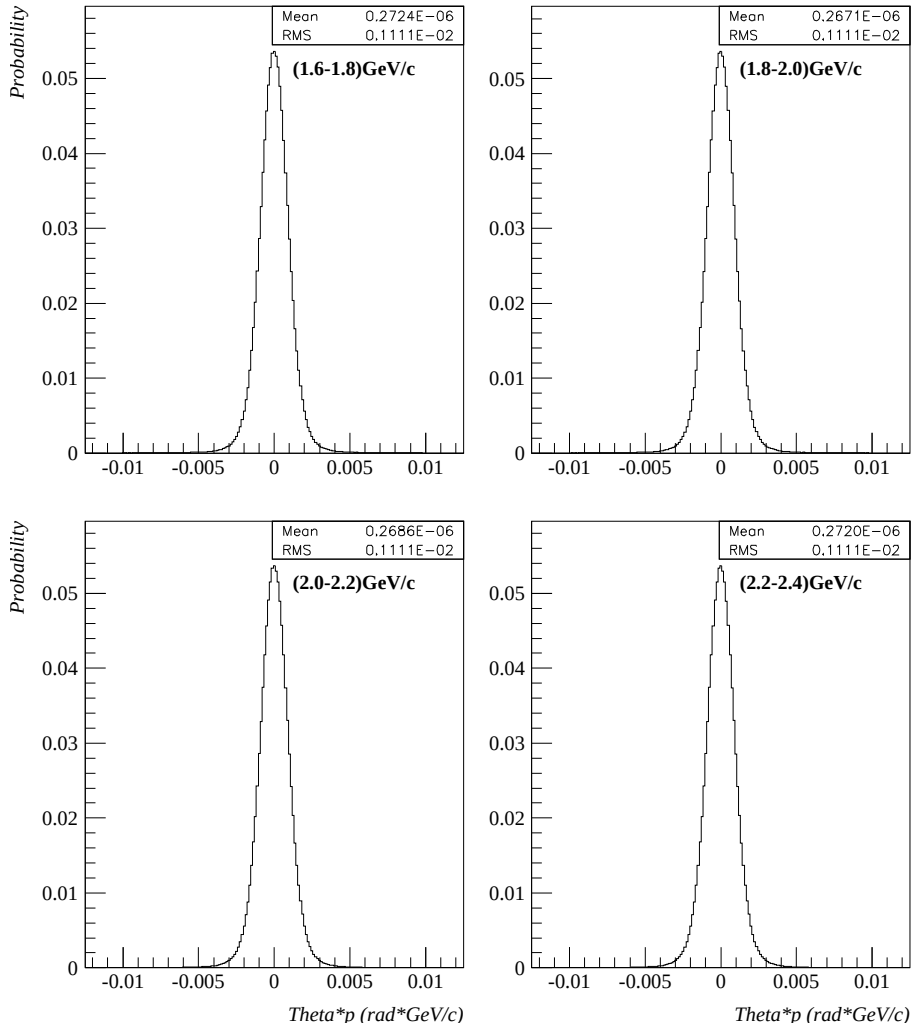

Figure 2: $\theta \times p$-dependence of the Moliere theory in Ni-sample for four momentum ranges.

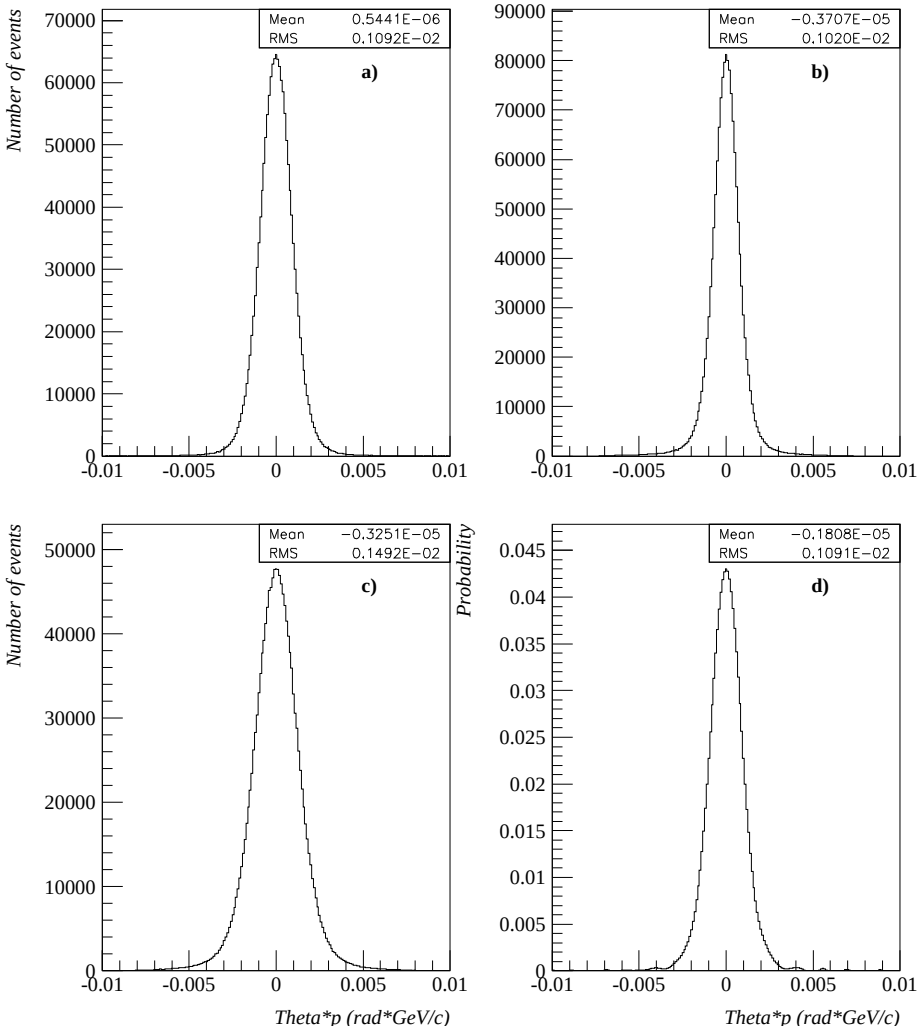

Figure 3: Ill-posed inverse problem solving for the Moliere distribution in Ni-sample. a - original multiple scattering distribution; b - drift chamber resolution; c - convolution of the a and b-distributions; d - reconstructed multiple scattering distribution.

3 Multiple scattering experimental data analysis

Fig. 4 illustrates typical experimental distributions (a and b) and result of the reconstruction procedure (c and d). It is needed to draw attention to some irregularities existing at the edges of reconstructed multiple scattering distribution (c-box). The value of this irregularity depends on available statistics and, of course, is less than the corresponding reconstruction error (d-box). Nevertheless, it is necessary to keep in mind this feature. For this reason it is incorrect to compare pure $R.M.S.$-values of reconstructed distributions.

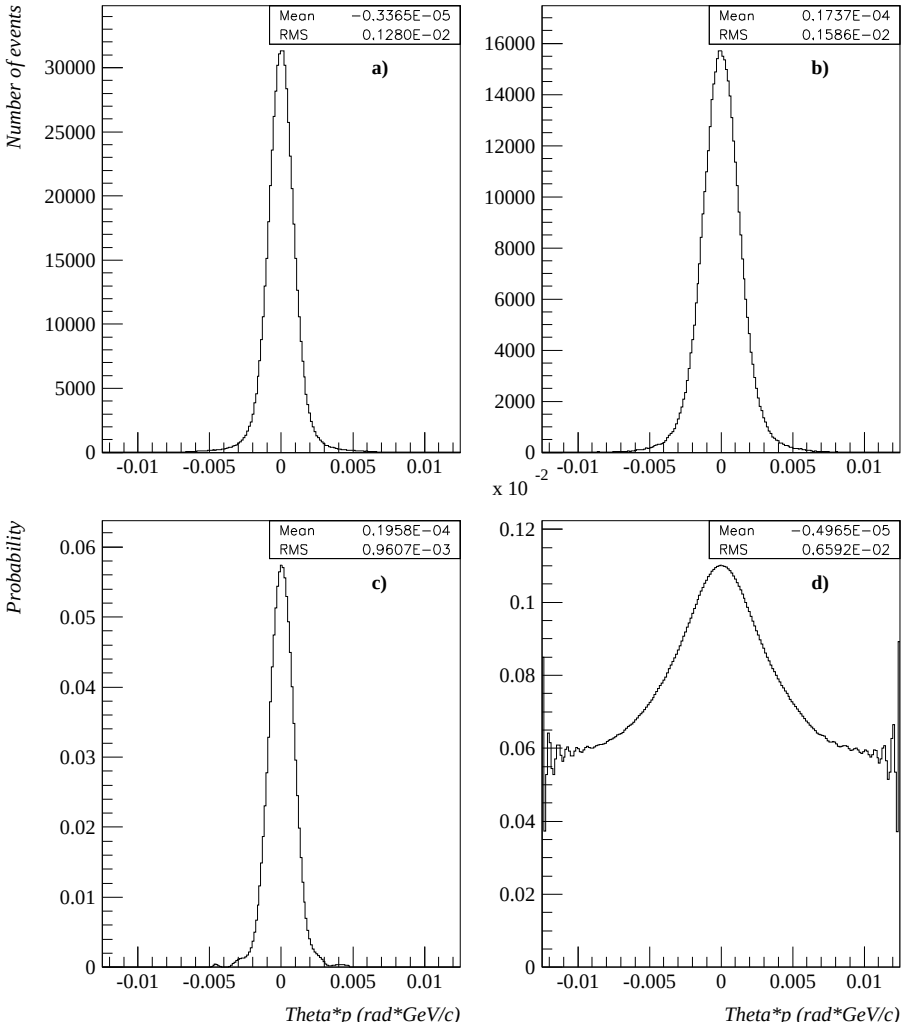

Figure 4: Ill-posed inverse problem solution for experimental data in Ni-sample. a - drift chamber resolution; b - distribution for particles which cross the Ni-sample; c - reconstructed multiple scattering distribution; d - reconstructed multiple scattering error distribution.

Fig. 5 is a complete analog of Fig. 2 and demonstrates p-independence of the $\theta \times p$-distributions for experimental data. As mentioned just above, the irregularity at the edges is rather visible due to small statistics. For comparison of these four distributions the Gaussian fit of the central part was made. The Gaussian $Sigma$-values are rather close to each other, taking into account small statistics.

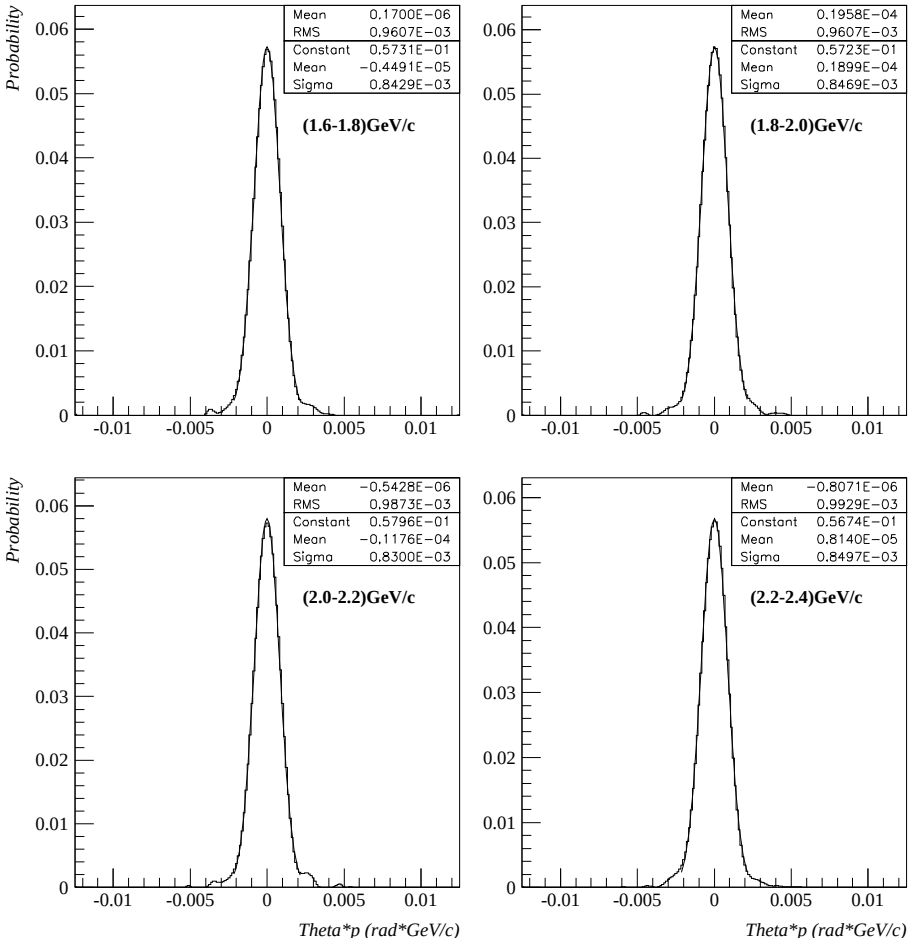

Figure 5: $\theta \times p$-dependence of the reconstructed multiple scattering in Ni-sample for four momentum ranges. Solid line is the Gaussian fit of the central part of the distributions.

4 Multiple scattering experimental data fit

Different functions to describe multiple scattering distribution were tested. Some of them give practically the same good description quality. Finally, a three-Gaussian mixture ($3G$) function (F) was chosen. The main advantage of this function consists in a simple way of summing the errors.

$$F(x) = N \times \left(c_1 \times \exp\left(-\frac{x^2}{2\sigma_1^2}\right) + c_2 \times \frac{\sigma_1}{\sigma_2} \times \exp\left(-\frac{x^2}{2\sigma_2^2}\right) + c_3 \times \frac{\sigma_1}{\sigma_3} \times \exp\left(-\frac{x^2}{2\sigma_3^2}\right)\right) \quad \text{, where} \tag{1}$$

$$\begin{aligned}
&x = \theta \times p \quad (rad \times GeV/c),\\
&N - \text{normalization factor},\\
&c_1 = \alpha_1 + \beta_1\sqrt{\frac{l}{X_0^*}} \quad , \qquad \sigma_1 = \gamma_1 + \delta_1\sqrt{\frac{l}{X_0^*}} \quad ,\\
&c_2 = \alpha_2 + \beta_2\sqrt{\frac{l}{X_0^*}} \quad , \qquad \sigma_2 = \gamma_2 + \delta_2\sqrt{\frac{l}{X_0^*}} \quad ,\\
&c_3 = 0.1c_2 \quad , \qquad \sigma_3 = 2.75\sigma_2 \quad .
\end{aligned} \tag{2}$$

X_0^*-parameter is, in a certain sense, an effective radiation length, which must be determined in such a way that it describes the particular multiple scattering distribution.

l is a sample thickness.

4.1 Ni data

Fig.6 shows reconstructed experimental multiple scattering distribution with error bars together with the 3G-function fit. Set of parameters, used in 3G-function is presented lower on this page. High quality of the fit is clear visible. Fit parameter P2 corresponds to the Ni-sample thickness and equals the true thickness value.

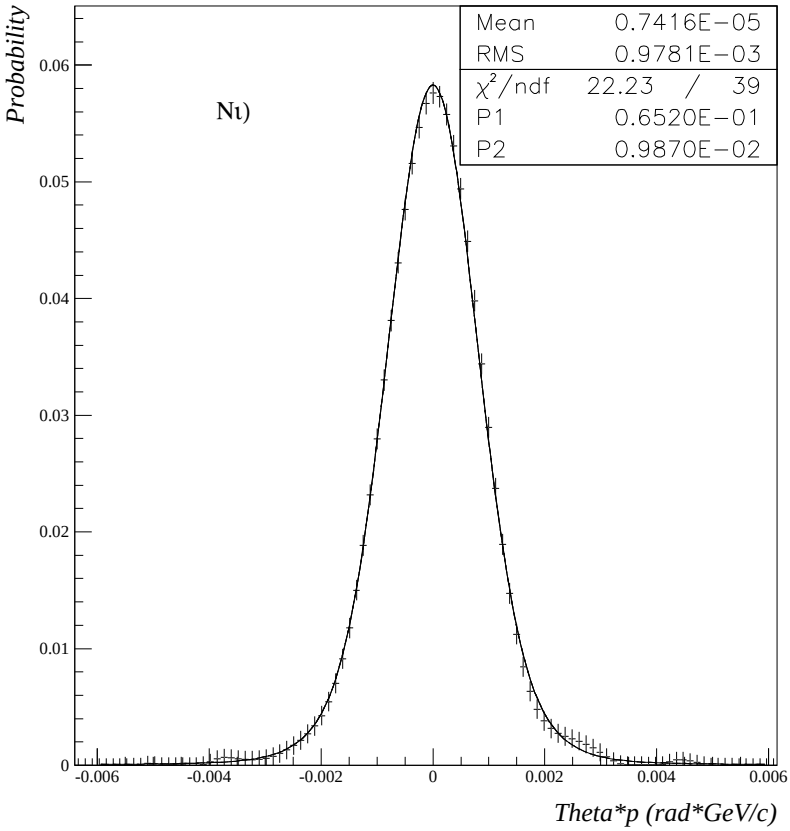

Figure 6: The 3G-function fit of the experimental multiple scattering distribution in the Ni-sample.

Set of parameters which are used in 3G-function (see formula 1):

$$\begin{aligned} \alpha_1 &= 0.692870\,, & \beta_1 &= 0.710858\ \ , \\ \alpha_2 &= 0.279209\,, & \beta_2 &= -0.646233\ \ , \\ \gamma_1 &= -0.913335 \times 10^{-4}\,, & \delta_1 &= 0.0110215\,, \\ \gamma_2 &= -0.938077 \times 10^{-4}\,, & \delta_2 &= 0.0172151\,. \end{aligned} \tag{3}$$

Effective radiation length equals X_0^*=1.63765cm which must be used instead of the standard value X_0=1.42336cm. Consequently, our measurement gives more narrow distribution than predicted by the standard Moliere theory.

4.2 Al data

Fig.7 shows reconstructed experimental multiple scattering distribution with error bars together with the 3G-function fit. Set of parameters, used in 3G-function is presented lower on this page. High quality of the fit is clear visible. Fit parameter P2 corresponds to the *Al*-sample thickness and equals the true thickness value.

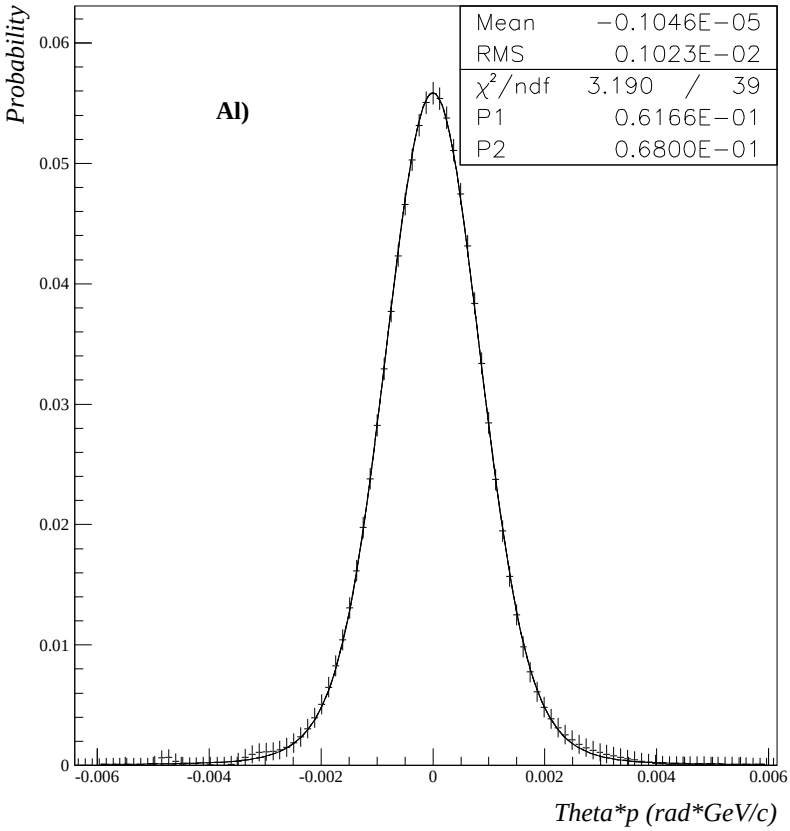

Figure 7: The 3G-function fit of the experimental multiple scattering distribution in the *Al*-sample.

Set of parameters which are used in 3G-function (see formula 1):

$$\begin{aligned} \alpha_1 &= 0.716504\,, & \beta_1 &= 0.566955\ \ , \\ \alpha_2 &= 0.257723\,, & \beta_2 &= -0.515414, \\ \gamma_1 &= -0.916234 \times 10^{-4}\,, & \delta_1 &= 0.0112173\,, \\ \gamma_2 &= -0.920313 \times 10^{-4}\,, & \delta_2 &= 0.0168419\,. \end{aligned} \tag{4}$$

These parameters are used also for $MSGC$-, SFD-X- and SFD-W-samples.

Effective radiation length, which must be used, equals X_0^*=10.6855cm instead of the standard value X_0=8.893cm. Consequently, our measurement gives more narrow distribution than predicted by the standard Moliere theory, as in case of Ni-sample.

4.3 MSGC data

Fig.8 shows reconstructed experimental multiple scattering distribution with error bars together with the 3G-function fit. Set of parameters, used in 3G-function is presented in section 4.2. High quality of the fit is clear visible.

Because the $MSGC$ structure is rather complicate, we did not try to describe the radiation length of the sample. Moreover, contrary to Ni and Al, it is not necessary for the DIRAC to have thickness dependence of the 3G-function. If to use radiation length of the glass $X_0^* = X_0 = 12.3cm$, then the fit parameter $P2$ corresponds to the $MSGC$-sample thickness $P2 = l = 0.0662468cm$, which is rather reasonable. Really, we must use the value $l/X_0^* = 0.538592 \times 10^{-2}$ for the simulation. The last comment is also valid to the SFD-X and SFD-W-samples.

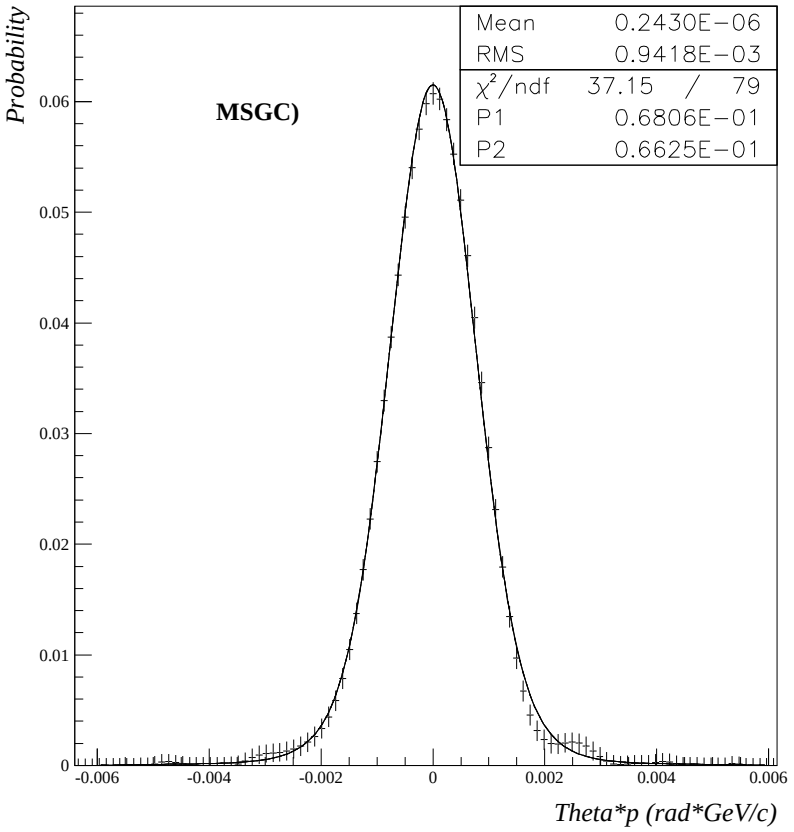

Figure 8: The 3G-function fit of the experimental multiple scattering distribution in the $MSGC$-sample.

4.4 SFD-X data

Fig.9 shows reconstructed experimental multiple scattering distribution with error bars together with the 3G-function fit. Set of parameters, used in 3G-function is presented in section 4.2. High quality of the fit is clear visible.

If to use the scintillator radiation length $X_0^* = X_0 = 42.4cm$, then the fit parameter $P2$ corresponds to the SFD-X-sample thickness $P2 = l = 0.353468cm$, which is rather reasonable. Really, we must use the value $l/X_0^* = 0.833651 \times 10^{-2}$ for the simulation.

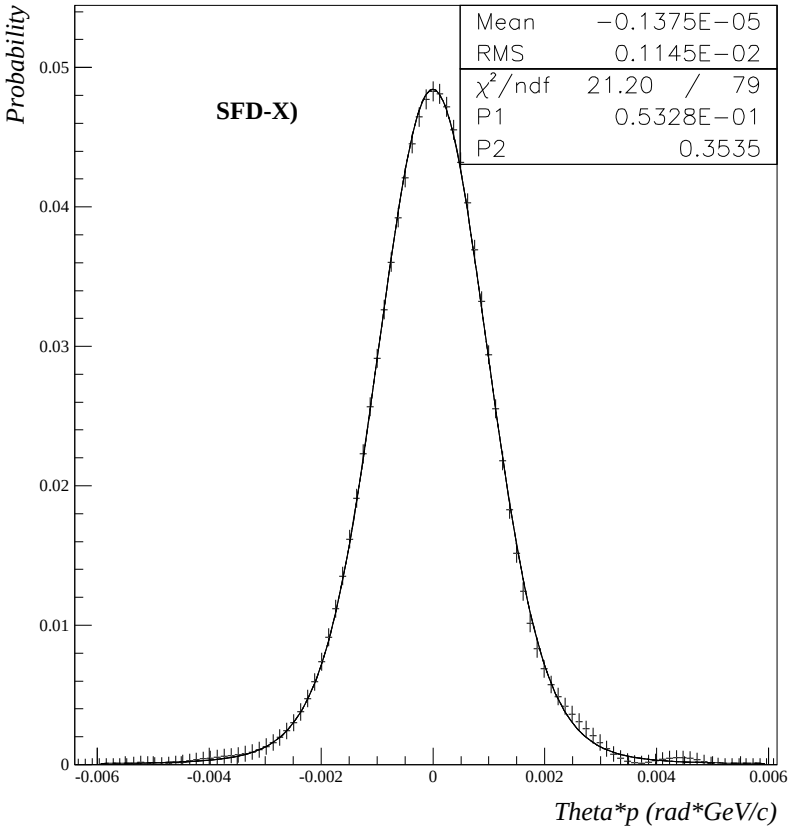

Figure 9: The 3G-function fit of the experimental multiple scattering distribution in the SFD-X-sample.

4.5 SFD-W data

Fig.10 shows reconstructed experimental multiple scattering distribution with error bars together with the 3G-function fit. Set of parameters, used in 3G-function is presented in section 4.2. High quality of the fit is clear visible.

If to use the scintillator radiation length $X_0^* = X_0 = 42.4cm$, then the fit parameter $P2$ corresponds to the SFD-X-sample thickness $P2 = l = 0.316869cm$, which is rather reasonable. Really, we must use the value $l/X_0^* = 0.747333 \times 10^{-2}$ for the simulation.

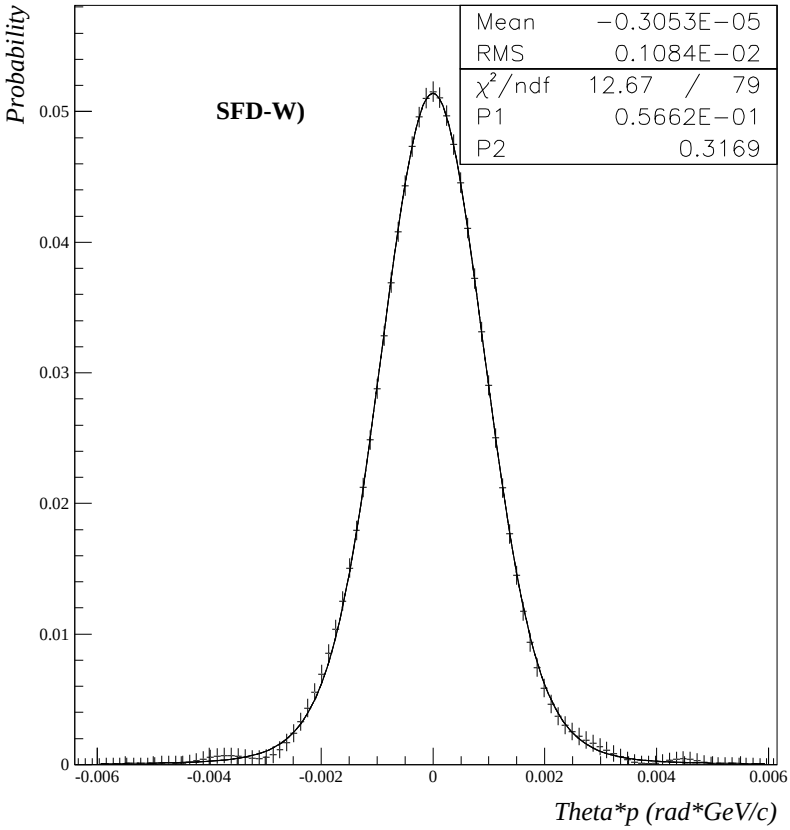

Figure 10: The 3G-function fit of the experimental multiple scattering distribution in the SFD-W-sample.

5 Conclusion

The formula(1) together with proper parameters presented in the note can be used for simulation of multiple scattering in the most important elements of the DIRAC setup. This formula describes the thickness dependence of the multiple scattering in the Ni-target and in the Al- window as well as in the whole $MSGC$, SFD-X and SFD-W detectors.